SPECIAL TOPIC — A 40th Anniversary Celebration: Physics Research and Innovation at Ningbo University

Molecular-group-assisted chemical precompression in superconducting molecular hydride $NaNH_{16}$

Daoyuan Zhang(张道远)[1,†], Xiang Wang(汪翔)[1,†], Tian Cui(崔田)[1,2,‡], and Zhao Liu(刘召)[1,§]

[1] *Institute of High Pressure Physics, School of Physical Science and Technology, Ningbo University, Ningbo* 315211, *China*
[2] *State Key Laboratory of Superhard Materials, College of Physics, Jilin University, Changchun* 130012, *China*

(Received 31 May 2026; revised manuscript received 24 July 2026; accepted manuscript online 17 August 2026)

Compressed hydrides have emerged as exemplary materials for high-temperature superconductivity, yet their experimental accessibility remains constrained by extreme pressure requirements (> 150 GPa) for obtaining atomic hydrogen structures. Here, we propose a strategy of incorporating the ammonium (NH_4) group into the molecular hydride NaH_{12} framework to enhance the chemical precompression effect and reduce the external pressure required for the stable structure. The resulting molecular hydride $R3$-$NaNH_{16}$ remains stable at a relatively low pressure of 20 GPa while preserving a high superconducting transition temperature of 54.5 K. Our first-principles calculations show that the added $NH_4^{+0.45}$ cation effectively regulates the charge distribution of surrounding hydrogen molecules, adjusting the hydrogen sublattice interactions through the hydrogen bond network, and forming a pseudo-binary hydrogen lattice. Compared with the parent NaH_{12}, $R3$-$NaNH_{16}$ exhibits stronger chemical precompression effects and structural stability at lower pressures. Further electron-phonon coupling analysis indicates that the bending vibrations of NH_4 and the translational-rotational modes of H_2 molecular units scatter nearly free electrons near the Fermi level, thereby forming Cooper pairs. Our results demonstrate that molecular doping into molecular hydrides to enhance chemical precompression provides a viable pathway to realize high superconductivity at low pressures.

Keywords: chemical precompression, molecular hydride, superconductivity, first-principles calculations

PACS: 74.70.Ad, 74.10.+v, 74.62.Fj

DOI: 10.1088/1674-1056/ae9a5f **CSTR:** 32038.14.CPB.ae9a5f

1. Introduction

Hydrogen-rich compounds have consistently attracted interest as promising platforms for phonon-mediated superconductivity owing to the extremely light mass of hydrogen and the resulting high characteristic phonon frequencies.[1–3] In such systems, superconductivity is predominantly driven by strong electron–phonon coupling (EPC) associated with hydrogen-dominated vibrational phonon modes. Over the past decade, this recognition has stimulated extensive theoretical and experimental efforts aimed at identifying superconductors with high superconducting transition temperatures (T_c) and understanding the microscopic mechanisms governing their superconducting behavior. Within this context, Ashcroft proposed the chemical precompression concept, which has emerged as a powerful and widely adopted framework for understanding and designing superconducting hydrides.[4] The central idea of chemical precompression is to introduce additional elements into lattices to modify the bonding characteristics of hydrogen, thereby reducing the external pressure required to stabilize superconducting states while preserving structural stability. Guided by this principle, a variety of atomic hydrides have been predicted and subsequently confirmed experimentally. Representative examples include H_3S[4–6] as well as rare-earth and alkaline-earth hydrides such as LaH_{10}, YH_9, and CaH_6[7–13] exhibiting T_c values exceeding 200 K under high pressures. Despite these remarkable advances with high-T_c, most of them remain stable only at ultrahigh pressures, typically exceeding 150 GPa, which poses severe challenges for experimental synthesis and limits their potential applications.[14–16] From the structural perspective, high-T_c superconductivity necessitates dense atomic hydrogen networks with extreme pressures to decompose molecular hydrogen and release free electrons, rendering low-pressure stabilization challenging.[17] These limitations highlight the necessity for alternative material design strategies that can stabilize superconducting hydrides at significantly lower pressures while maintaining strong EPC.

Currently, ternary hydrides have emerged as a significant approach within the conventional chemical precompression paradigm. By combining multiple metallic elements, introducing light nonmetal components, or engineering hydrogen-based alloy backbones, additional degrees of freedom can be introduced to tailor lattice symmetry, electronic structure,

[†]These authors contributed equally to this work
[‡]Corresponding author. E-mail: liuzhao@nbu.edu.cn
[§]Corresponding author. E-mail: cuitian@nbu.edu.cn

© 2026 Chinese Physical Society and IOP Publishing Ltd. All rights, including for text and data mining, AI training, and similar technologies, are reserved.

CPB Online Ahead of Press

and phonon vibration modes.[18–20] Notable examples encompass ternary AXH_8 compounds featuring fluorite-type alloy backbones, alkaline and rare-earth boron hydrides, as well as various rare-earth-based ternary hydrides that display tunable hydrogen sublattices and modified electronic states.[21–29] In these hydrides, the cooperative chemical effects between different constituents can significantly reduce stabilization pressures and, in some cases, further enhance T_c. These findings demonstrate that chemical precompression can be generalized to more complex chemical motifs and structural architectures. Apart from elemental substitution and alloying strategies, an emerging approach involves incorporating molecular functional groups into molecular hydride lattices. In contrast to isolated atomic dopants, molecular groups possess internal charge asymmetry. As a result, they can introduce additional electrostatic interactions that may improve lattice stability at reduced pressure. Moreover, our previous research has shown that alkali-metal and alkaline-earth-metal molecular hydrides, such as NaH_{12}, exhibit a high T_c of 154 K at 150 GPa.[30] However, the stability of molecular hydrides compressed with molecular groups and the microscopic mechanisms that influence superconductivity remain poorly understood. Thus, establishing clear relationships between molecular-group-assisted structures and superconductivity in molecular hydrides is essential for developing general design principles for low-pressure superconducting hydrides.

In this work, we propose a NH_4-group-assisted chemical precompression strategy for the molecular hydride NaH_{12} to reveal the correlation between chemical precompression and superconductivity. Here, we design a ternary molecular hydride $NaNH_{16}$, where NH_4 groups are periodically embedded between layers of molecular H_2. Our first-principles calculations demonstrate that $NaNH_{16}$ is both dynamically and thermodynamically stable at a markedly reduced pressure of 20 GPa, which is significantly lower than the pressure required to stabilize the parent NaH_{12}. Detailed electronic-structure and phonon analyses disclose that the incorporation of NH_4 groups leads to additional chemical precompression interactions. These include dihydrogen-bond contacts with neighboring H_2 units and weak interactions with the Na framework, which collectively strengthen the electrostatic stabilization of the system and contribute to chemical precompression. Moreover, these interactions give rise to low-frequency collective phonon modes that couple strongly with nearly free-electron hydrogen-derived states at the Fermi level, resulting in a superconducting transition temperature of 54.5 K. Our results demonstrate that molecular units can function as generalized chemical precompressors in molecular hydrides, thereby extending the traditional element-doping paradigm.

2. Calculational details

The Vienna *ab initio* simulation package (VASP) is utilized for DFT calculations, employing the projected augmented wave pseudopotentials (PAW) method[31] to accurately describe the electron-ion interaction. The $1s^1$, $3s^1 3p^0$ and $2s^2 2p^3$ were treated as valence electrons for elements H, Na, and N, respectively. The PBE of generalized gradient approximation (GGA)[32,33] has been employed as the exchange-correlation functional. The structural optimizations are conducted using the cutoff energy of 800 eV and the $8\times8\times8$ Monkhorst–Pack[34] $\boldsymbol{k}$-point grids, where the energy and force convergence criteria are set as 10^{-8} eV and -10^{-4} eV/Å, respectively. Weak interactions were analyzed using Multiwfn[35] based on single-point calculations performed with Gaussian (PBE/Lanl2DZ). The QUANTUM ESPRESSO package has been adopted to calculate the EPC and superconducting properties.[36] Ultrasoft pseudopotentials are used with a kinetic energy cutoff of 100 Ry. Self-consistent electron density and EPC are calculated by employing $16\times16\times16$ $\boldsymbol{k}$-mesh and $4\times4\times4$ $\boldsymbol{q}$-mesh for $NaNH_{16}$. In addition, the superconductivity is evaluated via the McMillan formula[37,38]

$$T_c = \frac{\omega_{\log}}{1.2}\exp\left(\frac{-1.04(1+\lambda)}{\lambda-\mu^*(1+0.62\lambda)}\right).$$

Here, $\omega_{\log}$ is the logarithmic average phonon frequency, μ^* is the Coulomb pseudopotential taken as 0.10, and λ is the total EPC parameter. The frequency-dependent EPC parameter λ is calculated by the Eliashberg spectral function $\alpha^2F(\omega)$

$$\lambda = 2\int \mathrm{d}\omega \frac{\alpha^2F(\omega)}{\omega},\quad \omega_{\log} = \exp\left(\frac{2}{\lambda}\int\frac{\mathrm{d}\omega}{\omega}\alpha^2F(\omega)\ln(\omega)\right).$$

3. Results and discussion

Inspired by the concept of chemical precompression, we introduce the NH_4 group into the reported molecular hydride R-3m-NaH_{12} prototype to construct a ternary hydride $NaNH_{16}$. After fully optimizing the structure at 20 GPa, the $R3$-$NaNH_{16}$ phase was obtained. The calculated enthalpy relations indicate that the synthesis pathway involving NH_4 doping is thermodynamically feasible. As depicted in Fig. 1(a), the ternary compound $NaNH_{16}$ exhibits negative formation enthalpies with respect to its constituent elements (Na, H, and N), relevant binary compounds, and reference reactions involving the NH_4 group over a wide pressure range from 10 GPa to 50 GPa. These results demonstrate that $NaNH_{16}$ is thermodynamically stable within this pressure interval. The optimized structure of $NaNH_{16}$ crystallizes into the space group $R3$ at 20 GPa, where Na, N, and H atoms occupy the Wyckoff position 1a. In the $R3$ phase, Na atoms with a coordination number of 8 occupy the vertices of the unit cell. On each face of the hexahedron, four H atoms with a coordination number of 2 are fixed and

CPB Online In-Press

form H_2 molecules in pairs, while the NH_4 group resides at the center of the lattice (Fig. 1(b)). In addition, the electrostatic energy of $NaNH_{16}$ is calculated to be −23.42 eV, which is much lower than that of NaH_{12} (−3.40 eV). After normalization, the electrostatic energy per unit volume of $NaNH_{16}$ is −0.284 eV/Å^3, while the corresponding value for NaH_{12} is −0.112 eV/Å^3, indicating that the $NaNH_{16}$ system exhibits stronger electrostatic interactions. This verifies the feasibility of introducing NH_4 as an effective chemical precompression strategy, as shown in Fig. 1(b).

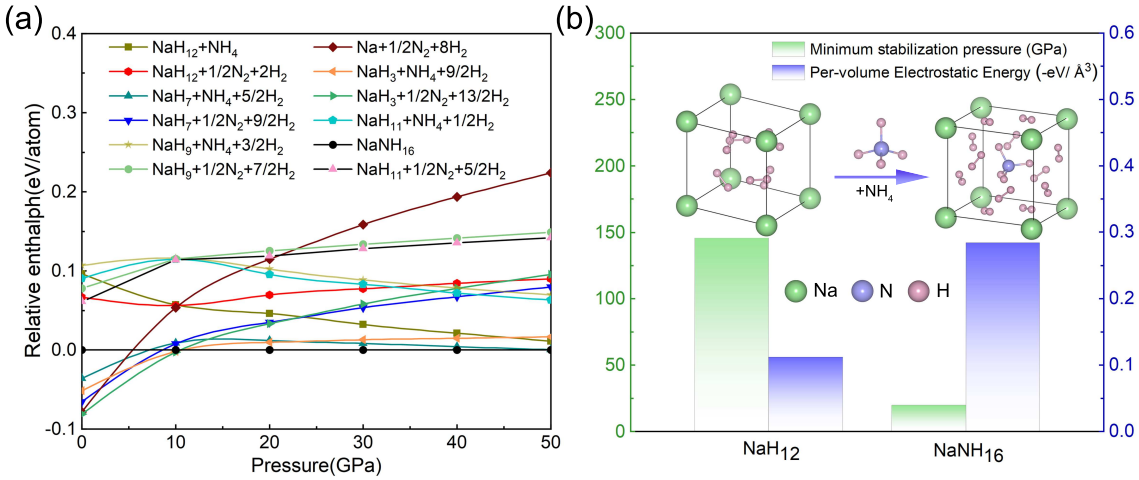


Fig. 1. (a) Formation enthalpies of various compounds and elements relative to $NaNH_{16}$.[39–42] (b) Schematic diagram of the formation of the *R*3 phase of $NaNH_{16}$ by incorporating an NH_4 group into the *R*-3*m* phase of NaH_{12}.

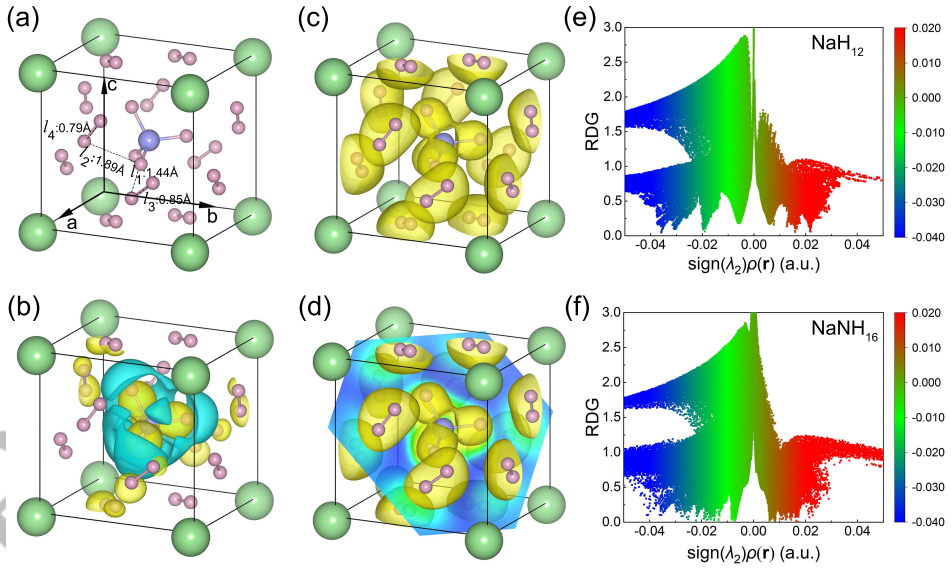


Fig. 2. (a) Structural schematic diagram of the *R*3-$NaNH_{16}$ phase at 20 GPa. (b) Differential charge density with an isosurface value of 0.008, where the cyan regions represent charge transfer and the yellow regions represent charge accumulation. Panels (c) and (d) present the 3D and 2D (1 1 1) electron localization function (ELF) schematic diagrams with an isosurface value of 0.75. Panels (e) and (f) show the scatter plots of the reduced density gradient (RDG) versus the electron density (ρ) for NaH_{12} and $NaNH_{16}$, respectively, where the data points are colored according to the sign of the second Hessian eigenvalue (λ_2).

The intriguing configuration of *R*3-$NaNH_{16}$ and the further chemical precompression resulting from the enhanced electrostatic potential motivated a deeper investigation into how the NH_4 group modulates the original hydrogen lattice. We first performed a detailed analysis of the lattice structure of $NaNH_{16}$. The distances between the H atoms (l_1) in the NH_4 unit and the surrounding H_2 molecules (l_2) were measured. The shortest l_1 distance is 1.44 Å, whereas the longest l_2 distance is 1.89 Å. It is worth noting that the bond length of the molecular H units near the NH_4 group (l_3: 0.84 Å) is noticeably longer than that of the molecular H units away from the group (l_4: 0.79 Å). This indicates that the incorporation of the NH_4 group effectively modulates the surrounding H_2 sublattice. To understand the nature of this modulation, we first performed Bader charge analysis to examine the charge transfer between atoms. The analysis reveals that within the NH_4 group, each H atom loses an average of 0.43 *e*, with a total of 1.27 *e* transferred to the central N atom. Together with the electron localization shown in Fig. 2(c) and the N–H COHP analysis in Fig. S2, these results confirm the polar

covalent nature of the N–H bonds within the NH_4 group. The differential charge density in Fig. 2(b) clearly shows distinct charge depletion in cyan regions around the periphery of the NH_4 group and charge accumulation in yellow regions around the H_2 molecules, providing further evidence for this charge transfer. This result explains why the total electrons lost by the Na atoms of 0.78 e and the NH_4 group of 0.45 e exactly equal the total electrons gained by H_2 molecules of 1.30 e. In this state, analysis of the 2D ELF on the (1 1 1) plane in Fig. 2(d) reveals delocalized electrons distributed around the NH_4 group with ELF values ranging from 0.25 to 0.45. These delocalized electrons originate from a small quantity of electrons transferred from both the NH_4 group and Na ions to the antibonding orbital σ^* of the H_2 molecules, resulting in slight ionization without causing complete dissociation. Moreover, the H atoms in the NH_4 group exhibit a positive partial charge, while the H_2 molecules overall carry a negative charge. The distance between the positively charged H atoms of NH_4 and the negatively charged H_2 molecules, denoted as l_1, is 1.44 Å, which is markedly less than the sum of the van der Waals radii of two H atoms of 2.40 Å. This implies a unique Coulomb interaction between the NH_4 group and the H_2 molecules, namely a dihydrogen bond $H^{\delta+}\cdots H^{\delta-}$.

The presence of dihydrogen bonds implies that the incorporation of the NH_4 group introduces additional weak interactions. We therefore performed reduced density gradient (RDG) analysis to quantify how the total weak interactions change upon incorporation of the NH_4 group. The RDG is defined as $\frac{1}{2(3\pi^2)^{1/3}}\frac{|\nabla\rho(\boldsymbol{r})|}{\rho(\boldsymbol{r})^{4/3}}$ and is plotted for NaH_{12} and $NaNH_{16}$ in Figs. 2(e) and 2(f). Here, $\rho(r)$ denotes the electron density, while the blue, green, and red regions correspond to attractive interactions, van der Waals interactions, and steric repulsion, respectively. In $NaNH_{16}$, the RDG distribution in the low-RDG region 0–0.2 exhibits additional weak-interaction features relative to NaH_{12}. The corresponding isosurfaces in Fig. S1 further show that, at an isosurface of 0.15, additional weak interactions emerge between the NH_4 units and Na atoms, whereas at an isosurface of 0.5, pronounced red RDG isosurfaces appear between adjacent molecular H_2 layers, together with distinct blue isosurfaces between the NH_4 units and neighboring H_2 molecules. These features indicate the presence of additional attractive noncovalent interactions between NH_4 and H_2, consistent with possible dihydrogen-bond contacts. These results indicate that the incorporation of the NH_4 unit significantly strengthens the Coulomb interaction and enhances the electrostatic stabilization of the system. The more negative electrostatic energy stabilizes a denser hydrogen sublattice, thereby providing electrostatic evidence for the chemical precompression effect.

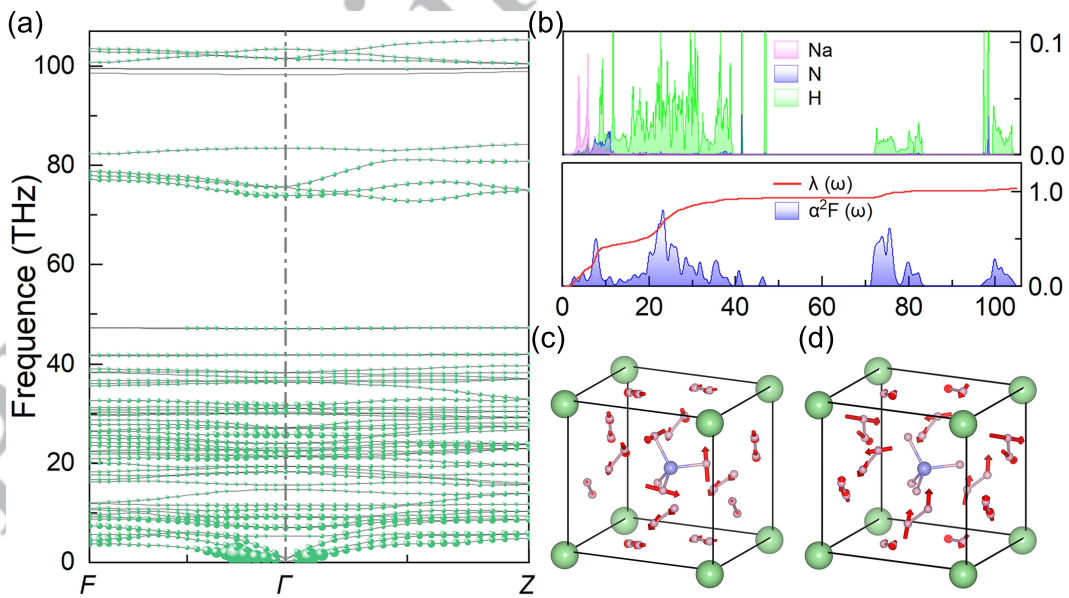


Fig. 3. (a) Phonon dispersion curve. (b) Phonon projected density of states, Eliashberg spectral function $\alpha^2F(\omega)$, and EPC parameter λ for $NaNH_{16}$ at 20 GPa. Panels (c) and (d) depict the atomic displacements of $NaNH_{16}$ at the Γ point at 7.8 THz and 23.2 THz, respectively.

To investigate whether the NH_4 group participates in the electron–phonon coupling of the system, we carried out a detailed lattice-dynamical analysis. The phonon dispersion and projected phonon density of states (PHDOS) reveal a pronounced low-frequency feature centered at approximately 7.8 THz. As evidenced by the atomic vibration schematic in Fig. 3(c), the phonon mode at 7.8 THz originates primarily from the bending vibrations of the NH_4 molecular units. In addition to this contribution, the Eliashberg spectral function $\alpha^2F(\omega)$ exhibits a distinct peak at approximately 23.2 THz, which also lies within the low-frequency phonon regime of $NaNH_{16}$. As indicated by the PHDOS, the contributions from Na and N atoms in this frequency range are negligible, confirming that this feature is primarily governed by hydrogen vibrations. Therefore, as shown in Fig. 3(d), these modes can be attributed to the coupled translational–rotational motions

of the H_2 molecular units, while the participation of the NH_4 group remains minimal. Together with the NH_4-related bending modes at lower frequencies, the coupled translational–rotational motions of the H_2 molecular units constitute the dominant low-frequency phonon modes of $NaNH_{16}$. Quantitative calculations of the EPC interaction reveal that phonon modes below 24 THz account for approximately 72% of the total EPC constant λ. The frequency-resolved projection of λ in Fig. 3(a) further corroborates that a substantial portion of the EPC strength originates from the low-frequency region. In contrast, phonons in the medium-to-high frequency region above 24 THz contribute only about 28% to λ. These results demonstrate that the superconductivity of $NaNH_{16}$ is primarily governed by low-frequency phonon modes, arising from the bending vibrations of NH_4 units and coupled translational–rotational motions of the H_2 molecular units.

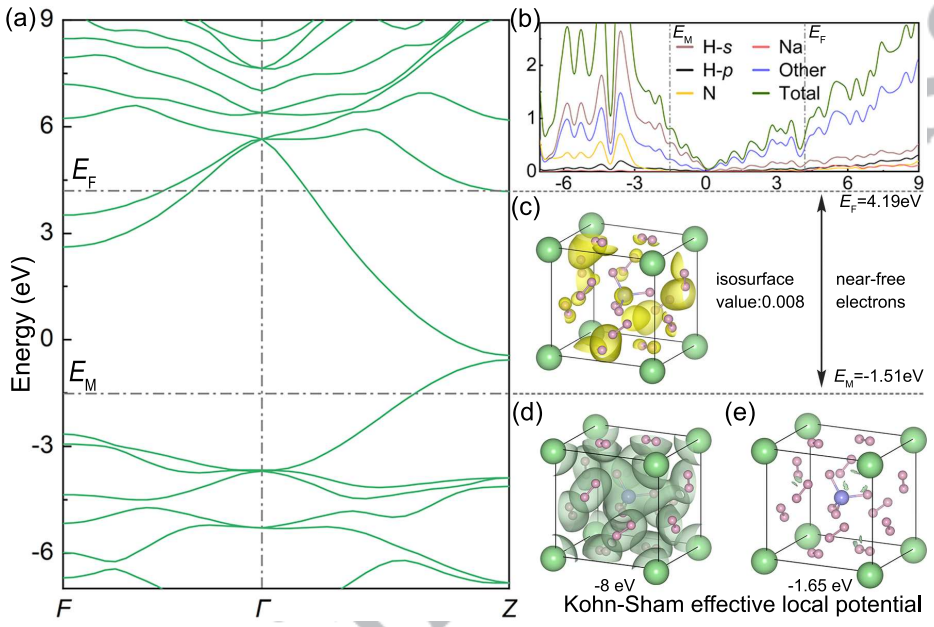


Fig. 4. (a) Band structure and (b) density of states (DOS) for $R3$-$NaNH_{16}$ at 20 GPa. (c) The 3D partial charge density maps with an isosurface value of 0.008. (d) and (e) The Kohn–Sham effective local potentials.

While the phonon analysis identifies the vibrational modes responsible for pairing, a complete understanding of the superconducting mechanism also requires examining the electronic states that couple to these modes. We therefore calculated the electronic band structure and density of states of $NaNH_{16}$. Examination of the projected DOS for this $R3$ phase indicates that the metallic bands at E_F are predominantly occupied by electrons from H-s orbitals. This is further corroborated by the band-decomposed plot in Fig. 4(c), which shows that the two degenerate bands just below E_F at approximately 4.19 eV are primarily composed of H-s orbital electrons from the molecular H_2. Therefore, it can be concluded that the metallicity of $R3$-$NaNH_{16}$ mainly originates from the H-s orbital electrons of the molecular hydrogen. To further confirm the contribution of these H-s orbital electrons to the superconductivity of the system, we calculated the Kohn-Sham effective local potential,[43] which incorporates the ionic potential, Hartree potential, and exchange-correlation potential, as shown in Figs. 4(d) and 4(e). At -8 eV, potential ridges emerge in the crystal interstices, connecting all atoms throughout the crystal. As the energy level increases, these ridges nearly vanish at -1.65 eV and completely disappear at -1.51 eV, where the maximum effective potential is located. The E_F at 4.19 eV is significantly higher than the maximum effective potential of -1.51 eV, indicating pronounced nearly free-electron behavior across the broad occupied state range from -1.51 eV to 4.19 eV. Analyzing these results in conjunction with those from Figs. 4(a) and 4(b), we demonstrate that the H-s orbital electrons near E_F exhibit nearly-free-electron behavior. Based on BCS theory and our analysis of the superconducting properties, the H-s orbital electrons at the Fermi level are identified as the dominant contributors to the electron–phonon coupling (EPC). We thus conclude that the low-frequency phonon modes are primarily associated with the bending vibrations of NH_4 units and the translational–rotational motions of H_2 molecular units, which scatter the H-s states with nearly free-electron behavior near the Fermi level to form Cooper pairs, thereby enabling superconductivity in this system. This electron–phonon coupling mechanism allows $NaNH_{16}$ to achieve a T_c of 54.5 K at the relatively low pressure of 20 GPa.

4. Conclusion

In summary, we have proposed and demonstrated a molecular-group-assisted chemical precompression strategy for stabilizing superconducting hydrides at reduced pressures.

By incorporating NH_4 molecular units into the NaH_{12} framework, we designed a ternary molecular hydride $NaNH_{16}$ that is dynamically and thermodynamically stable at a low pressure of 20 GPa and exhibits a superconducting transition temperature of 54.5 K. Detailed charge, bonding, and reduced-density-gradient analyses indicate that the incorporation of NH_4 introduces additional weak noncovalent interactions, including dihydrogen-bond interactions with neighboring H_2 molecules and weak interactions with the Na lattice. These interactions further enhance the electrostatic stabilization of the system and, from an electrostatic perspective, support a stronger chemical precompression effect, thereby helping to rationalize the superior stability of $NaNH_{16}$ relative to its binary parent NaH_{12} at lower pressures. Phonon and electron–phonon coupling calculations further show that superconductivity in $NaNH_{16}$ is dominated by low-frequency molecular vibrational modes. Quantitative analysis indicates that phonons below 24 THz contribute approximately 72% of the total electron–phonon coupling constant λ, with the dominant contributions arising from bending vibrations of the NH_4 groups and coupled translational–rotational motions of the H_2 molecular units. Electronic structure calculations and Kohn-Sham effective potential analysis reveal that the states near the Fermi level are dominated by H-s orbital electrons with free-electron-like character, which are scattered by low-frequency phonons to form Cooper pairs, thereby enabling superconductivity. These results highlight the crucial role of molecular units in simultaneously tuning lattice stability, vibrational spectra, and electron–phonon coupling. Our work establishes molecular groups as effective generalized chemical precompressors and provides new insights into the design of low-pressure superconducting hydrides through the cooperative interplay of electrostatic interactions and low-frequency lattice dynamics.

Acknowledgments

Project supported by the National Key Research and Development Program of China (Grant No. 2023YFA1406200), the National Natural Science Foundation of China (Grant No. 12304021), the Zhejiang Provincial Natural Science Foundation of China (Grants No. MS26A040028), the Natural Science Foundation of Ningbo (Grants Nos. 2022J091 and ZX2025001430), the Program for Science and Technology Innovation Team in Zhejiang (Grants No. 2021R01004), and the Program for Changjiang Scholars and Innovative Research Team in University (Grants No. IRT15R23). The calculations were performed in the Supercomputer Center of Ningbo University.

References

[1] Ashcroft N W 2004 *Phys. Rev. Lett.* **92** 187002
[2] Ma L, Wang X, Zhang Y, Liu H, Chen J, Zhao K and Yang W 2025 *J. Am. Chem. Soc.* **147** 4375
[3] Lu K, Zhou M, Cheng X, Hong X and Sun Y 2024 *Natl. Sci. Rev.* **11** nwad241
[4] Drozdov A P, Eremets M I, Troyan I A, Ksenofontov V and Shylin S I 2015 *Nature* **525** 73
[5] Duan D, Liu Y, Tian F, Li D, Huang X, Zhao Z, Yu H, Liu B, Tian W and Cui T 2014 *Sci. Rep.* **4** 6968
[6] Einaga M, Sakata M, Ishikawa T, Shimizu K, Eremets M, Drozdov A, Troyan I and Hirao N 2016 *Nat. Phys.* **12** 835
[7] Drozdov A P, Kong P P, Minkov V S, Besedin I S, Chernikova A A, Balicas L, Vinogradov N, Yaresko A, Tkalya E V and Eremets M I 2019 *Nature* **569** 528
[8] Peng F, Sun Y, Pickard C J, Needs R J, Wilkins J W and McMahon M I 2017 *Phys. Rev. Lett.* **119** 107001
[9] Liu H, Naumov I I, Hoffmann R, Ashcroft N W and Salvuzzi A R 2017 *Proc. Natl. Acad. Sci. USA* **114** 6990
[10] Somayazulu M, Ahart M, Mishra A K, Hemley R J, Hooper J F, Hoyt J J and Cohen M L 2019 *Phys. Rev. Lett.* **122** 027001
[11] Sun Y, Peng F, Zhang X, Pickard C J, Needs R J, Walter M J and McMahon M I 2019 *Phys. Rev. Lett.* **123** 097001
[12] Wang Y, Wang X, Zhang Z, Lin H, Liu H, Zhao J and Ma Y 2014 *J. Chem. Phys.* **140** 124707
[13] Ma X, Li J, Zhang J, Wang Y, Lv J, Liu H, Zhao Y and Ma Y 2022 *Phys. Rev. Lett.* **128** 167001
[14] Flores-Livas J A, Boeri L, Sanna A, Profeta G, Arita R and Gross E K U 2020 *Phys. Rep.* **856** 1
[15] Errea E, Calandra M and Mauri F 2020 *Phys. Rev. B* **102** 024524
[16] Tse J S 2017 *Annu. Rev. Phys. Chem.* **68** 273
[17] Zurek E and Bi T 2019 *J. Chem. Phys.* **150** 050901
[18] Zhang Z, Cui T, Hutcheon M J, Zeng Q, Wang X, Lin H, Liu H, Zhao J and Ma Y 2022 *Phys. Rev. Lett.* **128** 047001
[19] Song H, Zhang Z, Duan D, Li F, Tian F, Huang X, Yu H, Liu B, Tian W and Cui T 2019 *J. Phys. Chem. Lett.* **10** 2761
[20] Li S, Zhang Z, Song H, Li F, Tian F, Huang X, Yu H, Liu B, Tian W and Cui T 2022 *Phys. Rev. B* **105** 224107
[21] Gao M, Yan X W, Lu Z Y, Chen G Y, Wang J L, Ren W J, Sun J L and Zhang Y M 2021 *Phys. Rev. B* **104** L100504
[22] Di Cataldo S, Heil C, von der Linden W and Boeri L 2021 *Phys. Rev. B* **104** L020511
[23] Liang X, Bergara A, Wei X, Wang Y, Lv J, Liu H, Zhao Y and Ma Y 2021 *Phys. Rev. B* **104** 134501
[24] Di Cataldo S, von der Linden W and Boeri L 2020 *Phys. Rev. B* **102** 014516
[25] Song X, Yin K, Wang Y, Hermann A, Liu H, Lv J, Li Q, Chen C and Ma Y 2024 *J. Am. Chem. Soc.* **146** 13797
[26] Kuang F, Zhang L, Wang M, Liu Y and Chen X 2026 *Physica B* **727** 418288
[27] Yang W H, Li J K, Zhang T, Wang S and Liu P 2025 *Phys. Chem. Chem. Phys.* **27** 10838
[28] Geng N, Liu H, Wang Y, Zhang Z and Ma Y 2024 *Mater. Today Phys.* **44** 101443
[29] Yang F, Zhang C, Wang Y, Zhang J, Kong P, Li S, Chen F, Jin Y, Ju M and Gao K 2025 *Chin. J. Phys.* **95** 600
[30] Liu Z, Li J, Zurek E, Bi T, Zhang Y and Wang X 2024 *Phys. Rev. B* **109** L180501
[31] Blöchl P E 1994 *Phys. Rev. B* **50** 17953
[32] Perdew J P, Chevary J A, Vosko S H, Jackson K A, Pederson M R, Singh D J and Fiolhais C 1992 *Phys. Rev. B* **46** 6671
[33] Perdew J P, Burke K and Ernzerhof M 1996 *Phys. Rev. Lett.* **77** 3865
[34] Pack J D and Monkhorst H J 1977 *Phys. Rev. B* **16** 1748
[35] Lu T and Chen F 2012 *J. Comput. Chem.* **33** 580
[36] Giannozzi P, Baroni S, Bonini N, *et al.* 2009 *J. Phys.: Condens. Matter* **21** 395502
[37] McMillan W L 1968 *Phys. Rev.* **167** 331
[38] Allen P B and Dynes R C 1975 *Phys. Rev. B* **12** 905
[39] Song X, Yin K, Wang Y, Hermann A, Liu H, Lv J, Li Q, Chen C and Ma Y 2019 *J. Phys. Chem. Lett.* **10** 2761
[40] Otto J W, Porter R F and Ruoff A L 1989 *J. Phys. Chem. Solids* **50** 171
[41] Kassab E and Evleth E M 1987 *J. Am. Chem. Soc.* **109** 1653
[42] Baettig P and Zurek E 2011 *Phys. Rev. Lett.* **106** 237002
[43] Liu P, Zhuang Q, Xu Q, Cui T and Liu Z 2025 *Sci. Adv.* **11** eadt941

CPB Online First